# Synthesis of Cobalt Doped ZnO/$Co_3O_4$ heterostructures for Efficient methylene blue dye degradation application

**Degefa Bekele Yai**

**A Thesis Submitted to the Department of Applied Chemistry**

**College of Applied Natural science**

**In Partial Fulfillment of the Requirement for the Degree of Master's in Applied Chemistry (Industrial Chemistry)**

**Office of Graduate Studies**

**Adama Science and Technology University**

**December , 2025**

**Adama , Ethiopia**

# Synthesis of Cobalt Doped ZnO/$Co_3O_4$ heterostructures for Efficient methylene blue dye degradation application

Degefa Bekele Yai

Supervisor: Buzuayehu Abebe (Ph.D.)

A Thesis Submitted to the Department of Applied Chemistry,

College Applied Natural science

In Partial Fulfillment of the Requirement for the Degree of Master's in Applied Chemistry (Industrial Chemistry)

Office of Graduate Studies

Adama Science and Technology University

December, 2025

Adama, Ethiopia

## DECLARATION

I thus certify that this master's thesis, "**Synthesis of Cobalt Doped ZnO/$Co_3O_4$ heterostructures for Efficient methylene blue dye degradation application**," is entirely original with no parts submission for the award of any degree , diploma or certificate from any other university.All references to materials used in the study have been properly cited.

| Degefa Bekele | _____ | _____ |
|---|---|---|
| Name of student | Signature | Date |

**Recommendation of Advisors/ Supervisors:**

This certifies that Degefa Bekele prepared the thesis, "**Synthesis of Cobalt Doped ZnO/$Co_3O_4$ heterostructures for Efficient methylene blue dye degradation application**," under my supervision in order to partially fulfill the requirements for the Masters of Science degree in Applied Chemistry (Industrial Chemistry). After reviewing the thesis's final, revised form, I hereby propose that it be submitted to the department in compliance with academic criteria.

Buzuayehu Abebe (Ph.D.) _____

Major Advisor/Supervisor Signature Date

**APPROVAL SHEET**

We, the undersigned, have reviewed Degefa Bekele's thesis, "**Synthesis of Cobalt Doped ZnO/$Co_3O_4$ heterostructures for Efficient methylene blue dye degradation application,"** and have looked at the candidate during the open defense. This attests to the thesis' compliance with academic requirements and its approval as a partial fulfillment of the requirements for the Master of Science in Applied Chemistry (industrial chemistry) degree.

Buzuayehu Abebe (Ph.D.)
Major Advisor/Supervisor Signature Date

**Approval of Board of Examiners:**

The thesis "**Synthesis of Cobalt Doped ZnO/$Co_3O_4$ heterostructures for Efficient methylene blue dye degradation application**" submitted by Degefa Bekele's was assessed by the undersigned, who also looked at the candidate during the open defense.This attests to the thesis's compliance with academic requirements and its approval as a partial fulfillment of the requirements for the Master of Science in Applied Chemistry (Industrial Chemistry).

| | | |
|---|---|---|
| Chairperson<br>Dr.Hizkeal Tsade | Signature | Date |
| Internal Examiner | Signature | Date |
| Dr. Zewdu Bezu |  | 26/12/2025 |
| External Examiner | Signature | Date |

The authorized version of the thesis must be submitted to the Office of Postgraduate Studies (OPGS) via the Department Graduate Council (DGC) and School Graduate Committee (SGC) for final acceptance

| | | |
|---|---|---|
| Department head | Signature | Date |
| College Dean | Signature | Date |
| Office of Postgraduate Studies, Dean | Signature | Date |

## ACKNOWLEDGEMENTS

The best and foremost, I am deeply grateful to My God for granting me my hard working and health needed to complete this work . I extend my heartfelt appreciation to my a advisor, **Dr. Buzuayehu Abebe** for his consistent guidance ,insightful comments , and invaluable support throughout this research his mentorship was essential to the successful completion of this thesis . I would also like to thanks **Mr. Guta Amenu** for his encouragement and Dr Debebe for his technical support during experimental work . Finaly , I am sincerely thankful to my family for their unwavering love , patience and encouragement throughout my academic journey . their moral and emotional support has been a constant source of strength .

# TABLE OF CONTENTS

## LIST OF FIGURES

## LIST OF TABLES

**LIST OF ACRONYMS**

| | |
|---|---|
| AOPs | Advanced oxidation processes |
| CB | Conduction band |
| FT-IR | Fourier Transforms Infrared |
| MB | Methylene blue |
| NPs | Nanoparticles |
| PL | Photoluminescence |
| SEM | Scanning electron microscope |
| VB | Valence band |
| TEM | Transmission Electron Microscopy |
| FESEM | Field Emission Scanning Electron Microscopy |
| HRTEM | High Resolution Transmission Electron Microscopy |
| EDX | Energy Dispersive X-ray Spectroscopy |
| SAED | Selected Area Electron Diffraction |
| DRS- | Diffuse Reflectance Spectroscopy |
| UV-Vis | Ultra Violet –Visible Spectroscopy |
| XRD | X-ray diffraction |

**Abstract**

*Catalysis research has turned its attention to improving optical and charge transfer materials by combining doping and interfacial engineering. Cobalt-doped ZnO/CoO (CZnO) heterostructures were created in order to accomplish an effective photocatalytic process for the breakdown of methylene blue dye. Successful cobalt incorporation and heterojunction development were confirmed by XRD analysis, which showed changes in diffraction peaks and the appearance of distinctive Co3O4 peaks.The crystallite sizes for pure ZnO and the doped heterostructure were detected as* 26.3 nm and 10.7 nm, in the order given. *High-resolution TEM images showed sharp lattice patterns with d-spacings of 0.273 nm for ZnO and 0.241 nm for $Co_3O_4$, further verifying the interface formation. CZnO particles exhibited nanoscale dimensions ranging from 27 to 50 nm. Surface morphology analysis via FESEM and elemental mapping through EDX confirmed a uniform distribution of cobalt and the absence of impurities. UV-vis DRS technique indicated improved light absorption and a notable reduction in band gap energy upon cobalt doping, with indirect bandgaps of 3.05 eV for ZnO and 1.71 eV for CZnO. Photoluminescence (PL) spectra showed decreased emission intensity for CZnO, suggesting efficient charge separation at the heterojunction interface. The photocatalytic performance of CZnO showed a 4.5-fold increase in the degradation rate of methylene blue ($k = 0.141\ min^{-1}$) compared to pure ZnO ($k = 0.031\ min^{-1}$), attributed to enhanced optical and charge transport properties. The results confirm the potential of the porous CZnO heterostructure, prepared via a straightforward combustion method, for scalable photocatalytic applications.*

***Keywords:*** *Extrinsic defect; intent contact; optical property; combustion; photocatalysis*

# CHAPTER ONE

## 1. Introduction

### 1.1. Background of study

With the rising of stable and environmentally harmful organic contaminants are released into waterways, endangering aquatic systems and human health (Mohamed Reda et al., 2017). One of the dangerous organic pollutants utilised in many different sectors is methylene blue. One promising method of wastewater filtration is important for semiconductor oxides use to reduce organic contaminants (Naveenkumar et al., 2024). Through sophisticated oxidation processes, zinc oxide (ZnO and titanium dioxide ($TiO_2$) are best semiconductor metals for oxidizing living thing contaminants. One of the broad band-gap materials with great chemical stability, low cost, and non-toxicity is ZnO (Oukacha et al., 2024). However, a single ZnO photo-catalyst that have the recombination of electron and holes is highly efficient only under UV irradiation, has photo-corrosion properties, has a low surface area, and has low light absorption properties (Abebe et al., 2024; Alshaikh et al., 2021). Therefore, doping with extrinsic impurities and heterojunction engineering are essential modifying techniques for minimizing ZnO's disadvantages.

The ionic radius of cobalt ions (0.058 nm), a soft acid, is very close to that of zinc ions (0.060 nm), which allows cobalt to easily integrate into the ZnO lattice (Meky et al., 2025). Cobalt is incorporated into the ZnO lattice to modify its band gap and enhance its tendency to absorb Expanded light spectrum .(Yang et al., 2025). Doping with cobalt introduces tail states near the ZnO valence band, which not only reduces the band gap but also allows catalytic activation of nearly 40% of the solar energy received by Earth (Deshapriya & Munaweera, 2024). Furthermore, the production of the $Co_3O_4$-ZnO heterojunction, the d-d transition, and the sp-d strong exchange interaction improve the optical and charge transfer characteristics (Karpyna et al., 2024). The empty d-orbitals in the cobalt ion's electronic structure allow it to readily capture electrons within the ZnO structure and speed up electron transfer processes. (Meky et al., 2024). Through charge transfer, the $CoO_4$-ZnO heterojunction's construction also improves the catalytic property. Alshaikh et al. used the catalyst of the $CoO_4$/ZnO p-n junction to successfully oxidize ciprofloxacin. Photon-induced charge separation and band gap energy reduction were observed in this study (Alshaikh et al., 2021). It was detected that that the electron transport band in ZnO closely aligns with the lower energy electron band of $CoO_4$, promoting hole migration from ZnO to $CoO_4$ and electron migration in the opposite direction (Tien & Chen, 2023). Its electronically configured partially filled 3d orbitals give it

excellent charge transfer capabilities in addition to its band edge potential compatibility (Luo et al., 2025).

Co-precipitation was used in earlier research to create cobalt doped nanomaterials. Cobalt inclusion into the zinc oxide crystalline structure was verified by a change in XRD peaks towards higher angles. Three d-d transition peaks at longer wavelengths were identified by UV-vis DRS analysis, suggesting the development of intermediate energy levels inside the ZnO band gap. With the showing a pseudo-first-order-rate pattern and a maximum reaction constant of 0.0387 $min^{-1}$, these materials demonstrated enhanced photocatalytic degradation of ciprofloxacin. (Meky et al., 2025).the fabricated cobalt-doped ZnO quantum dots (QDs) for degrading methylene blue solution. The achieved a high degradation rate coefficient of 0.43 $min^{-1}$, attributed to cobalt doping and enhanced optical characteristics. Interestingly, the absence of cobalt peaks in the XRD patterns confirmed successful doping without forming separate cobalt phases (Chatterjee et al., 2023).

$Co_3O_4$/ZnO heterojunctions were created by Mohamed Reda et al. through the simple solid-state reaction method. As previously reported, the charge transfer reprocess was aided by the development of a $CoO_4$/ZnO heterojunction, which demonstrated a five-fold increase in degrading capability relative to single ZnO. The formation of distinct $Co_3O_4$ peaks in XRD patterns confirmed heterojunction formation. HRTEM analysis showed well-defined lattice fringes for ZnO (101) and $CoO_4$ (311) planes with d-spacing measures 0.248 nm and 0.244 nm, in the same order. (Mohamed Reda et al., 2017). Similarly, Alshaikh et al. employed a one-pot sol-gel method to synthesize $CoO_4$/ZnO materials for ciprofloxacin degradation. The materials demonstrated improved light absorption in the visible range and electron transfer due to the formation of a p-n heterojunction (Alshaikh et al., 2021). According to these literature reviews, in-depth studies have been conducted separately on cobalt doping in ZnO and on $Co_3O_4$/ZnO heterojunctions, very few reports explore the simultaneous formation of both in a single synthesis process. Furthermore, there are no detailed studies on cobalt-doped ZnO combined with $CoO_4$ heterostructures for degrading methylene blue dye.

To address this gap, the present work focuses on the production of a cobalt-doped with ZnO/$CoO_4$ (CZnO) heterostructure for the efficient breakdown of methylene blue. XRD analysis revealed both a peak shift (indicating cobalt incorporation) and distinct peaks corresponding to $Co_3O_4$ and ZnO, confirming lattice doping and heterojunction formation.

HRTEM analysis further validated the presence of individual ZnO and $CoO_4$ crystal phases based on measured d-spacing values. Enhanced optical properties, efficient charge separation, and broader light absorption were observed due to the combined effects of doping and heterostructure formation. UV-vis DRS revealed a narrowed band gap, while photoluminescence (PL) spectra displayed diminished emission , showing decreased recombination with enhanced carrier mobility. It is discovered that CZnO has a far higher capacity for degrading methylene blue dye than does single ZnO.

### 1.2. Statement of the problem

Here are some potential problem statements that could guide the r esearch was many. As the rise of textile industries the water was polluted .synthetic methylene blue dyes risk for human health and for a animals The synthesis of Co-doped ZnO/Co3O4 heterostructures was face challenges related to achieving uniform distribution, phase purity, and optimal morphology. The stability of the synthesized Co-doped ZnO/Co3O4 heterostructure under operational conditions (e.g., light exposure, pH, and temperature) will be critical for practical applications. The environmental implications of synthesizing and utilizing Co-doped $ZnO/Co_3O_4$ heterostructures for dye degradation were considered. There is a need for systematic comparative studies between Co-doped $ZnO/Co_3O_4$ heterostructures and other existing to catalysts to evaluate their effectiveness in methylene blue dye decline.

### 1.3. Objectives of study

#### 1.3.1. General objective

The general objective of this study is to synthesize and characterize Cobalt Doped doped $ZnO/Co_3O_4$ heterostructures for photocatalysis applications.

#### 1.3.2. Specific objectives

- To prepared $Co_3O_4$ and ZnO NPs
- To prepared Cobalt doped $ZnO/Co_3O_4$ HSs
- To characterize the synthesized NPs and heterostructures using best analytical methods such as XRD, DRS-UV-vis, PL, FTIR, and SEM.
- To analyze the methylene blue dye reduction capabilities of synthesized NPs and heterostructure nanomaterials.

### 1.4. Significance of the study

The studying the investigate of Co-doped ZnO/Co3O4 heterostructures for methylene blue dye reduction applications was articulated through several key points: Methylene blue is a common pollutant in wastewater, particularly from textile and dye industries. Investigating Co-doping in ZnO helps clarify the role of metal ion incorporation on the material's properties.The creation of heterostructures was enhance photocatalytic performance through synergistic effects between different materials.This study contributes to the growing field of heterostructured photo catalysts. If successful, this research was lead to the development of scalable synthesis methods for producing Co-doped ZnO/$Co_3O_4$ heterostructures.

The study was aligns with the rules of green chemistry by promoting the importants of photocatalytic processes to employ solar power to facilitate chemical changes . This approach reduces reliance on harmful chemicals and energy-intensive methods for dye degradation. Advancements in the synthesis and characterization of novel materials like Co-doped ZnO/$Co_3O_4$ heterostructures was contributed to the field of material science, paving the way for new discoveries Protect for human health and the use of nano materials are important for the synthesis of co-doped ZnO /Co3O4 hetrostructures

### 1.4. Scope of the study

The researcher presented in this thesis report focuses on the synthesis and characterization of Co-doped ZnO/Co3O4 hetrostructures aimed at enhancing catalytic activity for various chemical reactions. I investigate the Co-doping of zinc oxide (ZnO) wih Cobalt (Co) to create a synergistic effect that improves the catalytic properties of material. by combining ZnO with $Co_3O_4$ , a transition metal oxide known for its catalytic capabilities , the study explores the potential of this hetrostructure to facilitate reactions such as oxidation and reduction processs. Through a series of synthesis methods, including sol-gel techniques, various compositions and morphologies of the hetrostructure are developed and analyzed. Analytical methods such as X-ray Diffraction (XRD), Scanning Electron microscopy (SEM) and UV-Vis spectroscopy are employed to evaluate the structural and optical properties of the synthesized materials

# CHAPTER TWO

# 2. Literature review

## 2.1. Fundamentals of Doping and Heterojunctions

A crucial method in semiconductor technology is doping, which is the intentional introduction of impurity atoms into a host lattice to change its optical, chemical, or electrical properties. This method is essential for customizing materials for particular purposes, particularly in photocatalysis. Dopants can create new energy states in a semiconductor's bandgap, which can improve electrical conductivity and enable more effective charge transport, both of which are necessary for increased catalytic activity. (Karamat et al., 2024).

When two distinct semiconductor materials pare combined, heterojunctions are created, which have special electrical characteristics that can greatly improve catalytic performance. Heterojunctions can enhance charge separation and active site stability in catalysis, increasing the efficiency of a variety of processes. (Balapure et al., 2024). The ability to combine materials at the nanoscale enables the precise tuning of both electronic structure and morphology, which is highly desirable for a wide range of catalytic process (Khan et al., 2019).

ZnO nanoparticles can be produced using a variety of methods, including sol-gel processing, chemical vapor deposition, and hydrothermal synthesis. (Raha & Ahmaruzzaman, 2022). Because of its favorable band edge locations—its valence band is below the oxidation potential of oxygen and its conduction band is above the reduction potential of water—ZnO is especially effective among semiconductor materials, enabling effective redox reactions under radiation. There are several ways to create ZnO nanoparticles, including sol-gel processing, chemical vapor deposition, and hydrothermal synthesis. (Ali et al., 2024; Goncharuk et al., 2010).

The sol-gel method is the best method as a result of its straightforward procedure, cost efficiency, and tendency to manufacture materials within well-controlled size, morphology, and composition. This method typically results in ZnO nanostructures with high surface area and customizable properties, degrading their photocatalytic activity. (Irede et al., 2024). Different types of semiconductor heterojunctions—such as type-I, type-II, p–n junctions, and Z-scheme systems—are often employed to improve the separation and mobility of light

releasing electron-hole pairs. These heterostructures, along with their mechanisms for photoinduced charge transfer, are often illustrated schematically (Ren et al., 2020).

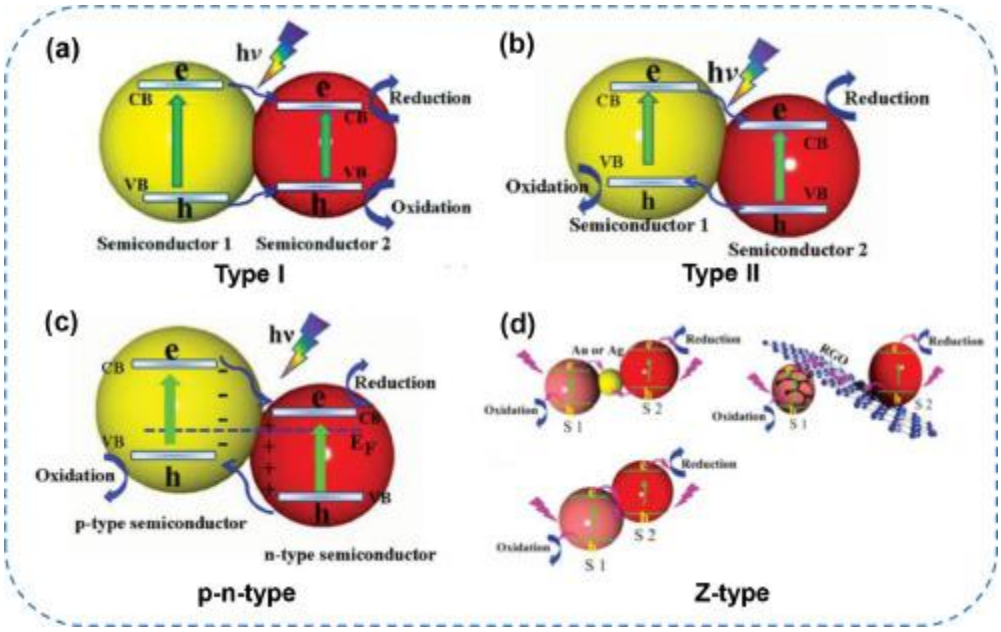


Figure 1. Schematic representations of heterostructure band alignments: (a) Type-I, (b) Type-II, (c) p–n junction, and (d) Z-scheme **configuration** (Ren et al., 2020).

### 2.2. Doping

Doping in semiconductors is generally classified into two types: n-type and p-type. In n-type doping, dopant atoms with more valence electrons than the base materials that are introduced, contributing free electrons that enhance conductivity. In contrast, p-type doping involves atoms with fewer valence electrons, resulting in the formation of electron-accepting "holes" that facilitate charge movement. (Wei et al., 2024). Beyond altering electrical properties, doping can also influence the physical characteristics of materials, including changes in surface morphology, generation of structural defects, and enhancement of surface area—all of which can significantly improve catalytic efficiency. (Barick et al., 2010; Leimane et al., 2025).

The choice of dopant is crucial, as it directly affects the semiconductor's performance. Transition metals such as cobalt (Co) are widely used in doping ZnO due to their ability to introduce intermediate energy levels within the bandgap. These new levels can serve as stepping stones for charge transfer, boosting reactivity and enhancing photocatalytic activity (Keshari et al.,
2021).

### 2.2.1. Cobalt-doped zinc oxide

Because it combines the inherent qualities of ZnO with the advantageous effects of cobalt doping, cobalt-doped ZnO (Co-ZnO) is of great interest in photocatalysis. The replacement process of Co ions into the ZnO lattice, which alters its electronic structure and is essential for efficient photocatalysis. (Singh et al., 2023). Several analytical techniques can be used to verify that cobalt ions are fully embedded in ZnO crystals. X-ray diffraction (XRD) techniques typically reveals a shift in diffraction peaks due to lattice distortion caused by the dopant. Additionally, UV-visible diffuse reflectance spectroscopy (DRS) often shows broader absorption bands at longer wavelengths, indicating enhanced visible light response and the presence of new energy levels associated with cobalt doping . (Ji et al., 2018; Kaphle & Hari, 2017), **as** illustrated in Figure 2a and 2b.

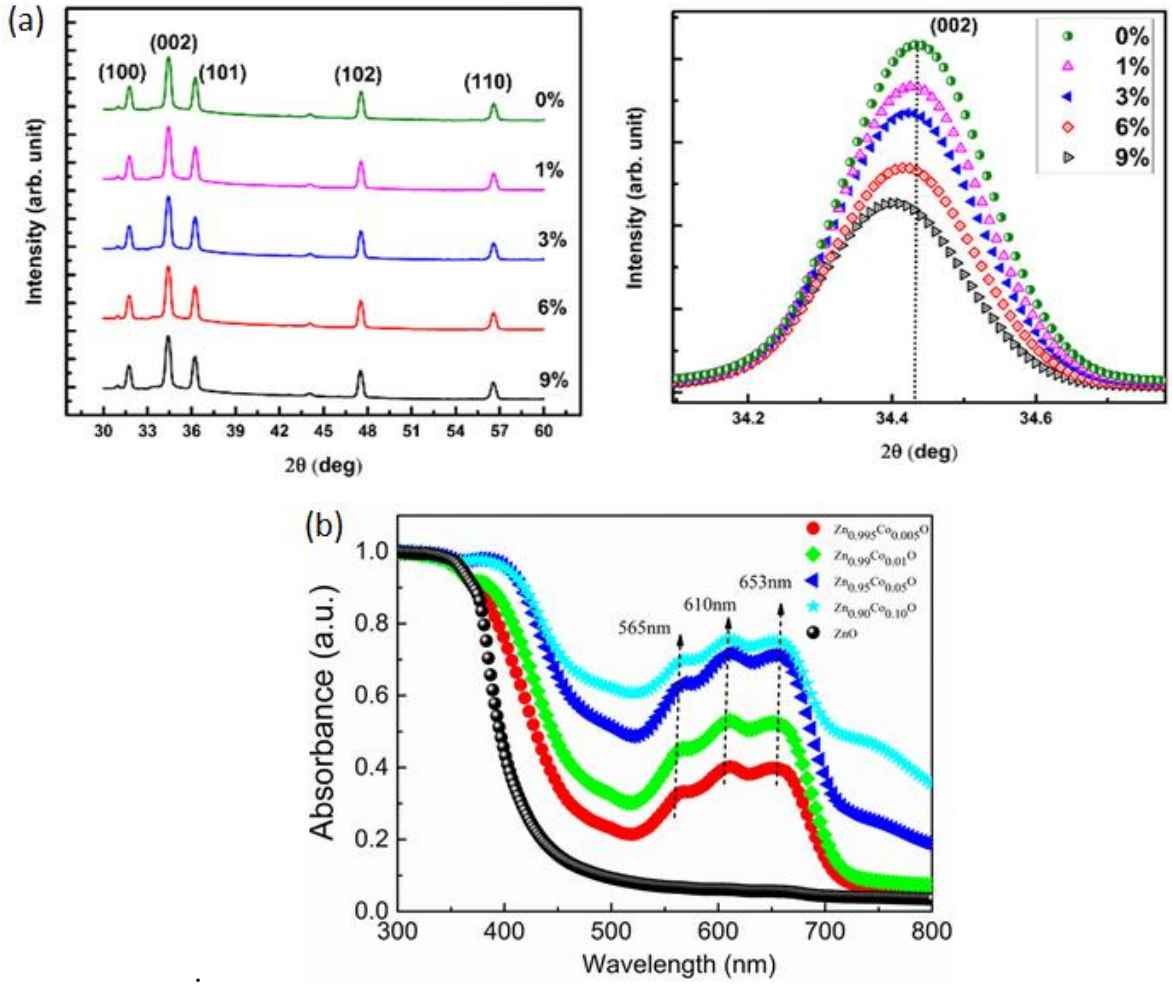


Figure 1. (a) XRD pattern and (b) the UV-vis spectrum Co-doped ZnO nanomaterials (Ji et al., 2018; Kaphle & Hari, 2017).

The sol-gel method is  used approach for fabricating Co-doped ZnO nanostructures due to its versatility in supporting  both the morphology and composition of the final material. This process involves dissolving metal precursors in a solvent to form a homogeneous sol, which then undergoes gelation. Subsequent thermal treatment transforms the gel into a crystalline material. Co-ZnO synthesized via this route typically exhibits improved photocatalytic performance, attributed to increased surface area and finely tunable structural properties . (Qu et al., 2025).

### 2.3. Cobalt-Doped Zinc Oxide/ Cobalt Oxide Heterostructures

The development of Co-ZnO/$Co_3O_4$ heterostructures via sol-gel methods represents a promising approach for enhancing catalytic performance in various reactions, including dye degradation applications such as methylene blue degradation. The formation of heterostructures allows for improved charge separation and stability, which are critical factors in catalytic efficiency. (Yakushova et al., 2025).

Research has shown that Co-ZnO/$Co_3O_4$ heterostructures manifest excellent catalytic reactivity relative to their alone  constituents. The incorporation of $Co_3O_4$ not only boosts the catalysts reactivity but also improves its durability and recyclability under working conditions.  (Markhabayeva et al., 2023). The mutually enhancing effect  between  ZnO and $Co_3O_4$ facilitates mor efficient charge shift and increases the density of catalytically catalytic region  .

Under light irradiation , the heterostructure undergoes photoexitation , where electrons are elevated to the higher energy band (CB) of ZnO, generating electron  hole in its lower energy band (VB). When ZnO and $Co_3O_4$ come into contact , their Fermi levels realign to reach equilibrium, forming  in the production of interface depletion layer . This occurs due to the movement of charge carrirs across the junction via both diffusion and drift process . following band alignment , electron generated in $Co_3O_4$ to ZnO, while holes migrate from ZnO to to $Co_3O4$ VB . this bidirectional charge separation happens naturally , without the need for external voltage and plays a crucial role in enhancing the photocatalytic efficiency of the hetrostructure. (Markhabayeva et al., 2023). This charge electron transfer techniques , illustrated in Figure 3, is key to the enhanced catalytic performance of the heterostructure.

.

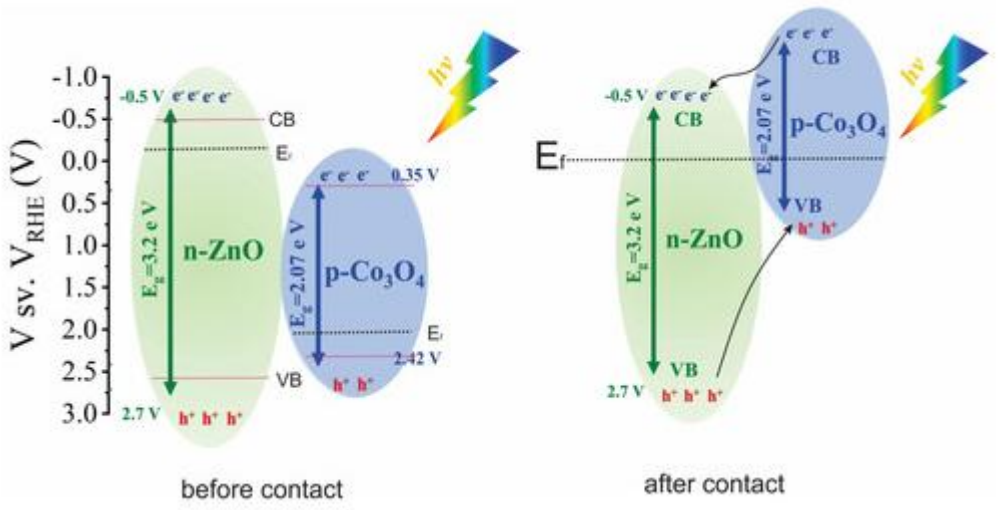


Figure 3. Schematic illustration of the ZnO/$Co_3O_4$ heterojunction and the associated charge transfer mechanism *(Markhabayeva et al., 2023).*

### 2.4. P-N Junctions

P–N junctions are interfaces produced between p-type and n-type semiconductors, resulting in a depletion region with distinct electronic behavior. These junctions are critical in various electronic and catalytic applications due to their ability to regulate charge carrier movement. In Co-ZnO/$Co_3O_4$ heterostructures, A p–n junction, which is formed at the interface of n-type ZnO and p-type $Co_3O_4$, is essential for enhancing charge carrier separation and transport . (Dagareh et al., 2024).

The p–n junction effectively facilitates the dissociation of light-induced electron –hole pairs, minimizing their recombination and reducing the lifetime and mobility of charge carriers.. This mechanism is particularly beneficial in catalytic applications where efficient charge transfer is essential for enhancing reaction rates. The presence of a p-n junction can lead to improved catalytic performance due to enhanced electron mobility and increased active sites for reactions. (Dagareh et al., 2024).

The production of Co-ZnO/$Co_3O_4$ heterostructures through sol-gel methods offers a pathway for developing efficient catalysts for methylene blue dye degradation. The unique properties

imparted by doping, combined with the advantages of heterostructuring and p-n junction formation, make these materials suitable for enhancing catalytic performance in environmental remediation processes . (Mohamed Reda et al., 2017). Based on the DRS UV-vis and Mott–Schottky plots analysis Nguyen et al. developed ZnO-$Co_3O_4$ heteojunction and charge transfer mechanism. Figure 4a Prior to contact, display the bandedgare potentials of ZnO and $CO_3O_4$. Following contact, ZnO's energy levels shift downward and $Co_3O_4$'s electronic state shift upward until their Fermi levels are equal. Consequently, as illustrated in Figure 4b, p–n junctions are created at the ZnO–$Co_3O_4$ contact, and electron transport takes place (Nguyen et al., 2024).

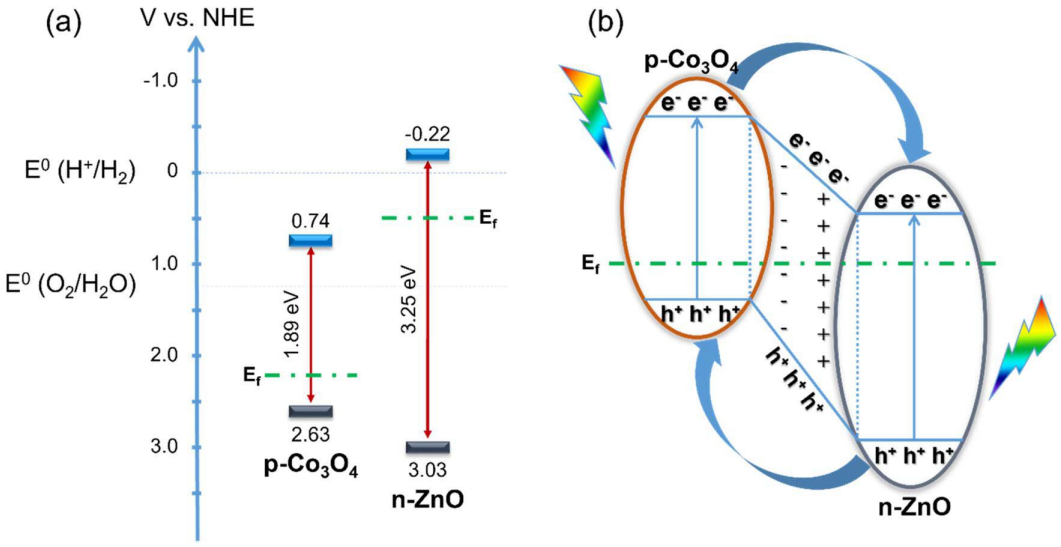


Figure 2. ZnO–$Co_3O_4$ heterojucnction mechanism befor (a) and after contact.

# CHAPTER THREE

## 3. Materials and Methods

### 3.1. Materials

The main metal precursors in the synthesis procedure were zinc nitrate with six water molecule [$Zn(NO_3)_2 \bullet 6H_2O$, 99.5% purity] and cobalt nitrate with six water molecule [$Co(NO_3)_2 \bullet 6H_2O$, 99.5% purity]. The capping and stabilizing ingredient was polyvinyl alcohol (PVA), which has a molecular weight between 85,000 and 124,000. Methylene blue dye is one example of a synthetic pollutant that has been used.

### 3.2. Synthesis of Nanomaterials

An easy sol-gel auto-combustion method was used to create the ZnO and CZnO materials. The synthesis experiment was carried out using several drugs and associated literature reports (Gao et al., 2016; Khort et al., 2021). In order to create ZnO NPs, the zinc nitrate with six water molecule was first dissolved in a PVA solution to form a homogeneous sol. The PVA was pre-dissolved in 75 mL of purified water under on going agitation at 80 °C using a magnetic agitation device to ensure complete dissolution (Liu et al., 2016). The mixture was then heated to 90–110 °C overnight to gradually remove water, resulting in the formation of a viscous gel complex. This gel was subsequently heated in an oven to its auto-ignition temperature (130–260 °C) to initiate combustion, yielding a foamy, porous intermediate. The resulting material was gently ground to reduce particle size and then thermally treat at 400 °C for one hour to get phase-pure ZnO dried gel nanoparticles.

The same method was adapted for synthesizing CZnO heterostructures, with the only difference being the inclusion of both zinc and cobalt nitrate salts in the precursor solution. After gelation and combustion, the product underwent calcination to produce the final Co-doped $ZnO/Co_3O_4$ material. Different doping levels were prepared by adjusting the molar ratio of cobalt to zinc precursors: 0.5%, 15%, 30%, and 45% Co, corresponding to 99.5%, 85%, 70%, and 55% Zn, respectively.

The resulting ZnO and CZnO materials were then subjected to detailed characterization and photocatalytic performance evaluation. The overall synthesis steps and photocatalytic testing strategy are illustrated schematically in Figure 5.

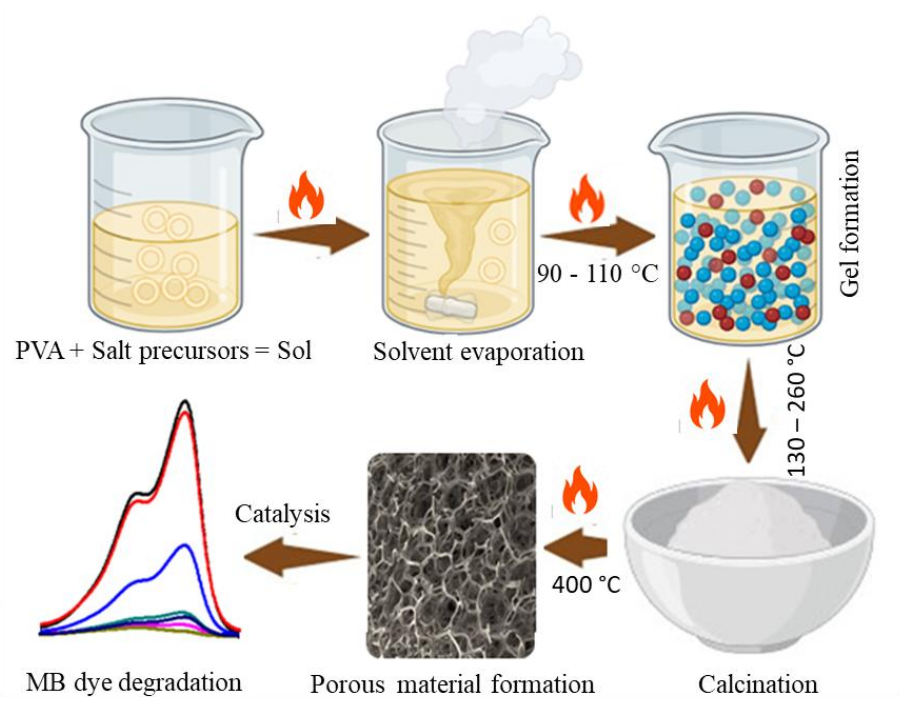


Figure 5: Overview of the Synthesis Method for CZnO Heterostructures and ZnO Nanoparticles

The synthesis process begins with dissolving metal salt precursors into a previously prepared polyvinyl alcohol (PVA) polymer solution. This mixture undergoes evaporation of the solvent to yield a PVA-starting gel. Upon heating, the gel reaches its auto-ignition temperature, initiating a combustion reaction. The combustion produces a porous xerogel powder, which is then subjected to calcination. The final product is subsequently utilized in experiments focused on the breakdown of methylene blue (MB) dye.

### 3.3. Materials Characterization Techniques

A variety of analytical methods served to analyze the produced nanomaterials' crystal and physicochemical characterstics : X-ray Diffraction (XRD): A SHIMADZU XRD-7000 diffractometer (Japan) was determined to the crystalline phases and structural characteristics. Scattered reflection in UV-Vis Spectroscopy (UV-Vis DRS): The energy differences were estimated and light absorption was determined through a Cary 100 UV-Vis spectrophotometer (USA). Photoluminescence (PL) Spectroscopy: Using 325 nm excitation, a Cary Eclipse fluorometer (Serial No.: MY18490002) was determined to examine the recombination kinetics of photoinduced conducting particles. Selected Area Electron Diffraction (SAED), High-Resolution TEM (HRTEM), and Transmission Electron Microscopy (TEM), Morphological features, lattice structures, and crystallinity were

examined using a JEOL TEM 2100 HRTEM (USA). Field Emission Scanning Electron Microscopy (FESEM) and Energy-Dispersive X-ray Spectroscopy (EDS): Surface topography and elemental composition were analyzed with a ZEISS SIGMA VP FESEM (Germany) integrated with an EDS system.

### 3.4. Photocatalytic Activity

The photo-reactive catalytic properties of undoped ZnO and Co-doped ZnO (CZnO) nanoparticles were evaluated in a 300 mL batch illumination reactor operating at a solution pH of 10. A 10 mg/L methylene blue solution was the target contaminant. For each experiment, 10 mg of the catalyst was mixed into the dye liquid mixture and agitated for 30 minutes in the absence of light to allow adsorption–desorption equilibrium. Following this dark phase, the solution was exposed to illumination to start the photocatalytic activity. Samples were taken every ten minutes, and the molarity of methylene blue was measured using a UV-Vis spectrophotometer. The pseudo-first-order model, which is represented by the : $\ln(Ct/Co) = -kt$, where Ct is the concentration of the dye at time t, Co is the starting concentration, at initial time and k is the rate constant. This model was used to compare the catalytic performance of the materials.

# CHAPTER FOUR

## 4. Results and discussion

### 4.1. Analytical characterization techniques

#### 4.1.1. XRD analysis

X-ray diffraction (XRD) was used to examine the solid state lattice and compute the crystalline particle size of the produced ZnO and Co-doped ZnO (CZnO) materials, as shown in Figure 6(a). The diffraction peaks matched those of ZnO's hexagonal wurtzite structure, which corresponds to JCPDS card number 004-0783. Diffraction peaks were found at 2θ values of 31.7° (100), 34.3° (002), 36.2° (101), 47.5° (102), 56.5° (110), 62.8° (103), and 67.9° (112), indicating the wurtzite phase. At lower cobalt doping levels, the CZnO samples showed diffraction patterns comparable to those of pure ZnO, showing that the wurtzite structure was retained . However, when the cobalt dopant concentration exceeded 15%, additional peaks attributed to $Co_3O_4$ appeared, suggesting the formation of a secondary phase. The presence and intensification of these $Co_3O_4$ peaks with increasing dopant levels indicate the coexistence of a ZnO–$Co_3O_4$ heterojunction. These peaks were found to match the reference pattern JCPDS No. 042-1467, confirming the crystalline nature of the $Co_3O_4$ phase. The emergence of these distinct $Co_3O_4$ peaks (marked by black dots in the figure) supports the formation of interfacial contact between ZnO and $Co_3O_4$ domains. A closer look at the XRD patterns in the magnified view (Figure 6(b)) reveals a slight shift in the diffraction peaks of CZnO relative to pure ZnO. This change can be ascribed to lattice distortion caused by the substitution of $Zn^{2+}$ ions (ionic radius: 0.060 nm) with $Co^{2+}$ ions (ionic radius: 0.058 nm), which introduces lattice contraction due to the smaller size of cobalt ion (Meky et al., 2025; Vieii et al., 2025). This change can be explained by lattice distortion brought about by replacing $Zn^{2+}$ ions (ionic radius: 0.060 nm) with $Co^{2+}$ ions (ionic radius: 0.058 nm). The smaller size of the cobalt ion causes lattice contraction. The Scherrer equation was used to estimate the samples' average crystallite size (D). The ($D = K\lambda/(\beta \cos \theta)$) was used to determine the average crystalline particle size . where λ is the X-ray radiation wavelength (0.15406 nm), β is the peak's full width at half maximum (FWHM), θ is the Bragg's angle of diffraction, and D is the average crystallite size. K is a dimensionless constant, usually 0.94 for spherical crystal shapes (Domingues et al., 2024).

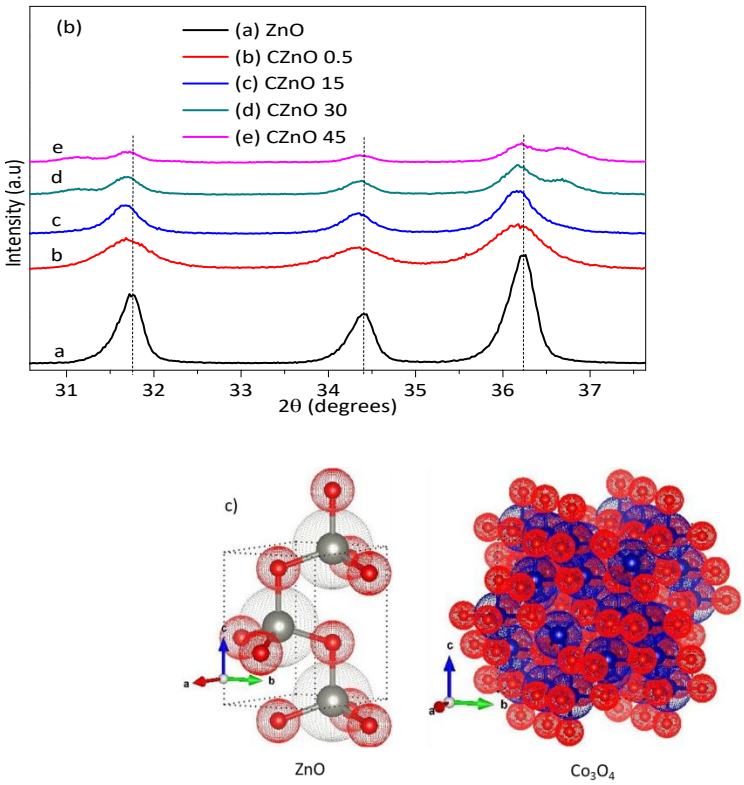


Figure 6: X-ray diffraction is used to investigate phase composition and crystal structure: (a) XRD pattern plots of ZnO NPs and 0.5, 15, 30, and 45% cobalt doped zinc oxide heterostructures; (b) a magnified image of the XRD pattern of ZnO NPs and CZnO heterostructures; and (c) the stable ZnO and $CoO_4$ crystal structure derived from the CIF data in the American Mineralogist Crystal Structure Database.

.

### 4.1.2. DRS UV-vis

To assess the light related behavior of the produced samples , UV–Vis diffuse reflectance spectroscopy (DRS) and photoluminescence (PL) analyses were performed. These techniques confirmed the modifications in light absorption and energy transitions resulting from cobalt ion incorporation and heterojunction formation. As seen in Figure 7(a), pure ZnO nanoparticles display a strong absorption peak at approximately 380 nm, a typical feature associated with their bandgap absorption. In comparison, Co-doped ZnO (CZnO) samples exhibited broader absorption and a noticeable red shift, indicating enhanced visible light absorption. The observed decrease in reflectance intensity in CZnO suggests improved light-harvesting capabilities due to cobalt doping. Additionally, in the 500–700 nm range, three subtle wave length –specific absorption appeared in the CZnO spectrum, attributed to d–d

transitions of cobalt ions within the ZnO lattice. (Akhtar et al., 2023). These transitions confirm the successful substitution of $Zn^{2+}$ with $Co^{2+}$ and imply that cobalt ions occupy tetrahedral coordination sites, consistent with ZnO's wurtzite crystal geometry (Vieii et al., 2025). Additionally, Akhtar et al. found that ZnO's bandgap shrinks as a result of the development of positive correction above the VB and negative correction below the CB (Akhtar et al., 2023). the introduction of Co ions causes positive energy level shifts above the valence band and negative corrections below the conduction band , effectively reducing the bandgap. This was further validated through bandgap calculations using the Kubelka–Munk function plotted against quantum energy , where linear extrapolation of the curve's tangent to the x-axis provided an estimate of the optical bandgap (Figure 7(b)).

The estimated bandgap energy for pure ZnO was 3.05 eV, while that of CZnO was significantly reduced to 1.71 eV. Since ZnO is inherently a direct bandgap semiconductor, its conduction band minimum and valence band maximum share the same crystal momentum (k-value), allowing for direct recombination of charge carriers and efficient light emission (Belay et al., 2023). Nonetheless, new mid-energy levels and with cobalt ions incorporated into the ZnO help electrons relax prior to recombination. As a result, potent pollutant-oxidizing species like hydroxyl radicals can be created when the electron –hole pairs produced by light combine with air and liquid water . However, the formation of intermediate energy levels due to cobalt doping offers additional relaxation pathways for electrons before recombination. These energy states extend the time span of charge carrier stability and enhance interaction with surrounding molecules. This mechanism promotes the creation of reactive radicals oxygen species (ROS), such as hydroxyl radicals, when photogenerated electrons and holes react with water and dissolved oxygen. The material is ideal for photocatalytic applications since these species are very good at breaking down organic contaminants. These oxidizing species facilitate the reactive breakdown of impurities on the catalytic surface.

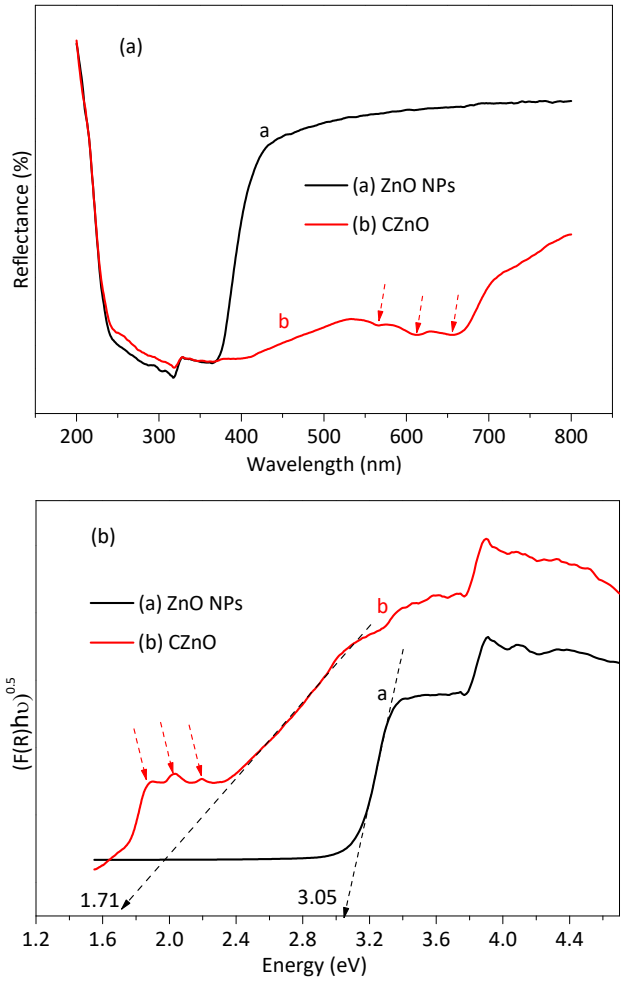


Figure 7. Optical characterization of ZnO and CZnO materials: (a) UV–Vis diffuse reflectance spectra (DRS), and (b) corresponding bandgap estimation using Kubelka–Munk plots.

### 4.1.3. PL

Figure 8: shows the photoluminescence (PL) spectra of cobalt-doped ZnO (CZnO) heterostructures and undoped ZnO at an excitation wavelength of 325 nm. The first near-band edge emission (NBE) of ZnO NPs was seen at 390 nm. A little shift in CZnO's NBE emission towards higher wavelengths is linked to the bandgap lowering. Naturally, changes in crystal quality are thought to be the cause of this shift. Additional emission peaks were found at roughly 422 nm, 443 nm, and 484 nm, which are often associated with inherent defects such as oxygen vacancies and zinc interstitials. (Chatterjee et al., 2023). When the gas byproduct changes during combustion reactions, several flaws may arise. In comparison to ZnO's intensityAs the dopant concentration rose, the CZnO PL spectra revealed virtually little quenching intensity. This intensity decrease is linked to the electron-hole recombination barrier, which encourages amplification in the charge transfer process. (Yang et al., 2025).

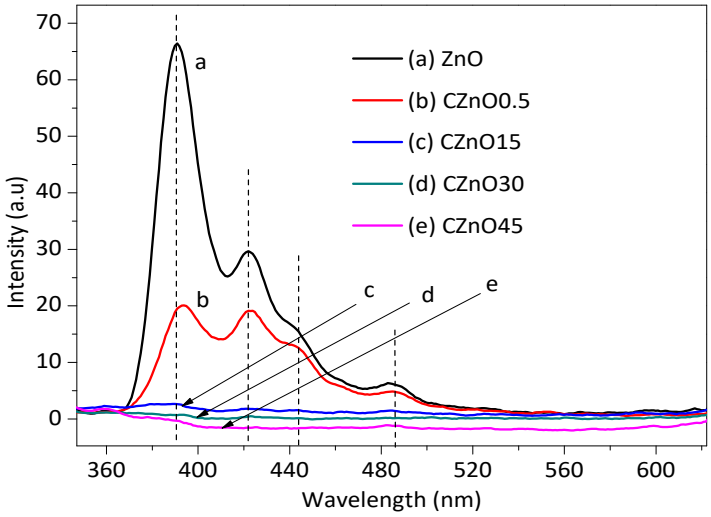


Figure 3: PL investigation of optical properties for ZnO and CZnO materials: the percentages of cobalt dopant are 0.5, 15, 30, and 45. ZnO NPs and 0.5, 15, 30, and 45 heterostructures are denoted by the inset labels a, b, c, d, and e, respectively.

### 4.1.4. FTIR

Figure 9 shows the FTIR spectra of samples of cobalt-doped ZnO (CZnO) and pure ZnO, which display broadly comparable vibrational properties but differ in intensity, peak position, and the appearance of extra bands in CZnO. The ZnO lattice's stretching vibrations are responsible for a significant absorption band about 450 $cm^{-1}$. O-H stretching vibrations from hydroxyl groups and adsorbed water molecules on the surface are responsible for the broad absorption peaks at 1660 $cm^{-1}$ and 3310 $cm^{-1}$. (Deshapriya & Munaweera, 2024). The $CO_2$ surface absorption is linked to the faint stretching band that was found in the 2300–2200 $cm^{-1}$ regions. The carbonyl group vibration is the cause of the band seen at about 1400 $cm^{-1}$ (Naveenkumar et al., 2024). **).** In the CZnO samples, several distinct absorption features appear in the 1050–1850 $cm^{-1}$ region. These are highlighted in Figure 9 with red arrows and are primarily attributed to the presence of secondary cobalt oxide phases, such as CoO and $Co_3O_4$, which may form alongside ZnO during synthesis (Deshapriya & Munaweera, 2024). Furthermore, the presence of the cobalt ion in the ZnO lattice is confirmed by the possibility that these distinct bands are caused by the Co-O bending vibration (Akhtar et al., 2023). The shift toward higher wavenumbers in the CZnO spectra is indicative of local bonding environment changes, likely caused by the shorter bond length of Co–O compared to Zn–O. This structural disruption further confirms the successful incorporation of cobalt ions into the ZnO matrix (Meky et al., 2024; Wachs, 1996).

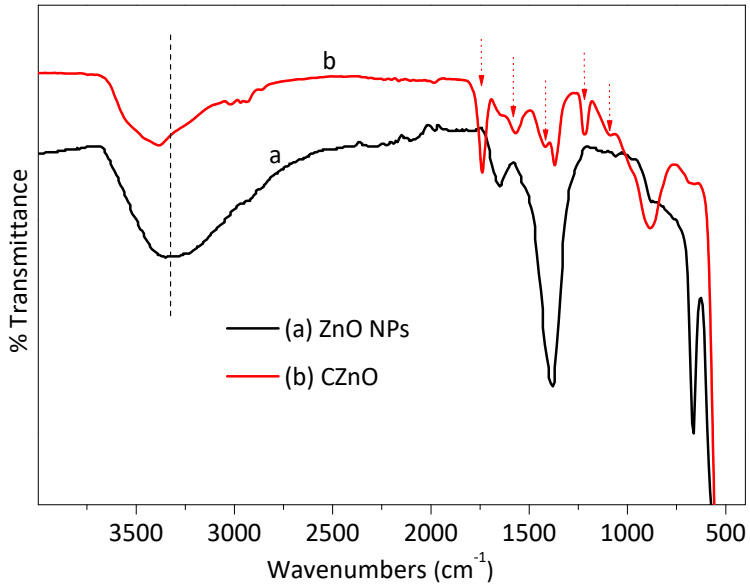


Figure 4: ZnO NPs and CZnO heterostructure FTIR spectra.

### 4.1.5. Morphological and compositional analysis

Figure 10(a) displays the surface morphology of the produced ZnO nanoparticles (NPs), whereas Figure 12(a) displays the Co-doped ZnO (CZnO) field emission scanning electron microscopy (FESEM) picture. In contrast to the rather homogeneous morphology of pure ZnO, the CZnO material exhibits a significant increase in particle aggregation. This phenomena can be explained by the creation of tiny cobalt (II, III) oxide particles., which possess higher surface energy, thereby promoting clustering during synthesis. Similar observations of enhanced aggregation and morphological transformation—often resulting in irregularly shaped particles—have been reported in recent studies (Akhtar et al., 2023; Meky et al., 2024, 2025). The form change was brought about by the ZnO crystal's elongation along the vertical axis. Figure 12(b) illustrates the well-dispersed cobalt dopant on the ZnO host surface using EDS layered elemental distribution. Figure 12(I) displays the electron image that was used to generate the EDS layered elemental distribution image. The elemental maps of cobalt, oxygen, and zinc are shown in Figures 12 (II, III, and IV). The EDS layered elemental distribution image of ZnO NPs is displayed in Figure 10(b), and the electron image used to create the EDS layered elemental distribution image is displayed in Figure 10(I). Additionally, elemental maps of zinc and oxygen are shown in Figures 10 (II and III).

.

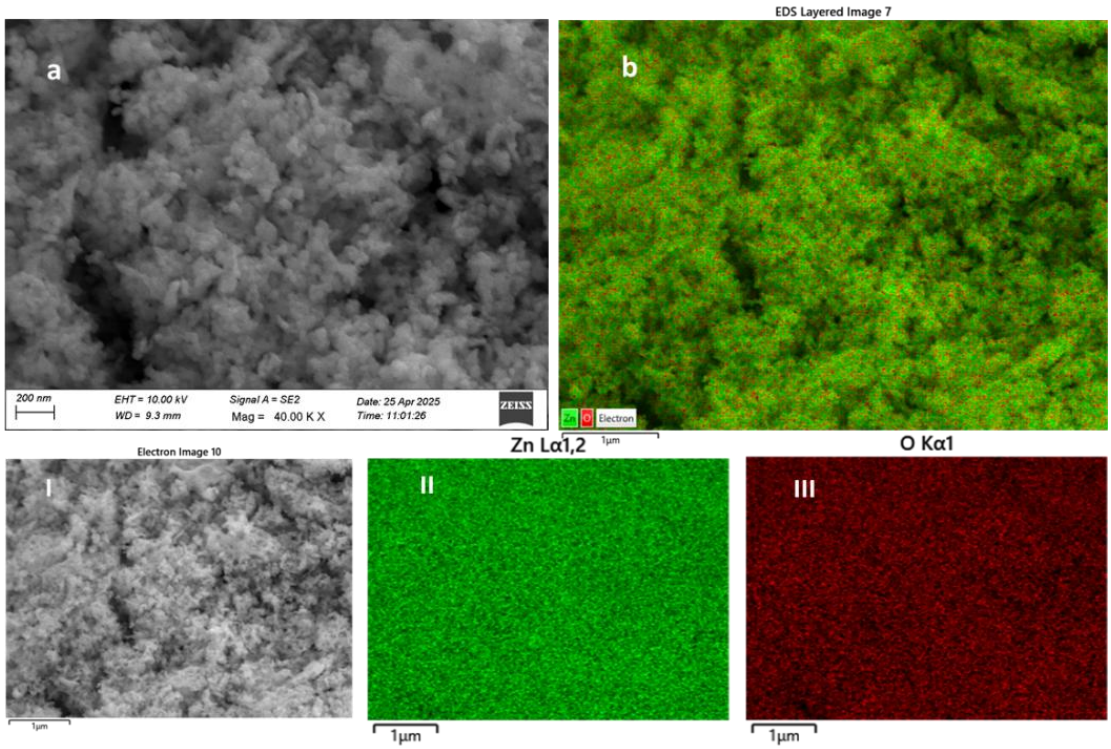


*Figure 5:* ZnO NPs material microscopic morphological analysis: (a) FESEM micrograph displaying surface structure; (b) EDS elemental distribution map; (I) matching electron image utilized for EDS mapping; and (II and III) elemental mapping of zinc and oxygen, respectively

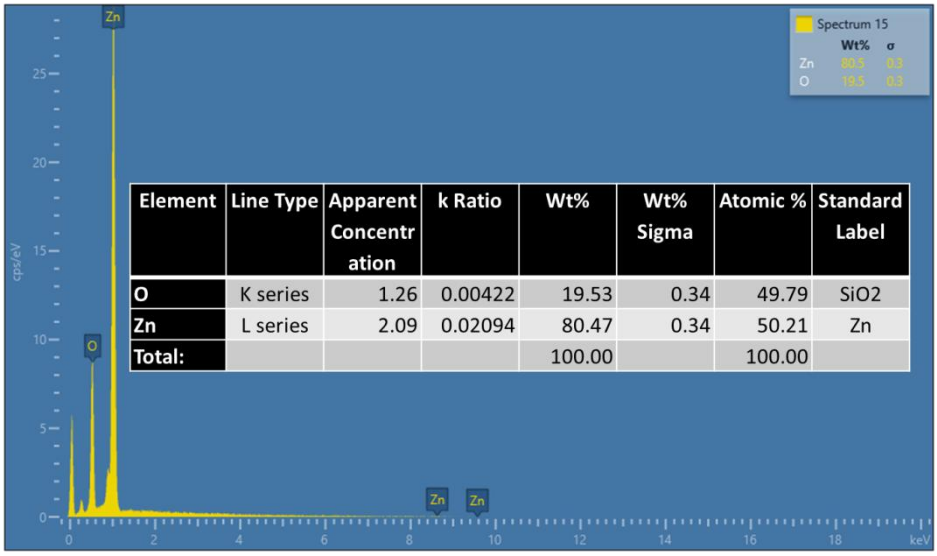


| Element | Line Type | Apparent Concentration | k Ratio | Wt% | Wt% Sigma | Atomic % | Standard Label |
|---|---|---|---|---|---|---|---|
| O | K series | 1.26 | 0.00422 | 19.53 | 0.34 | 49.79 | SiO2 |
| Zn | L series | 2.09 | 0.02094 | 80.47 | 0.34 | 50.21 | Zn |
| Total: | | | | 100.00 | | 100.00 | |

Figure 6: ZnO NPs' EDX elemental composition analysis spectrum; the comprehensive compositional analysis findings are shown in the inset table.

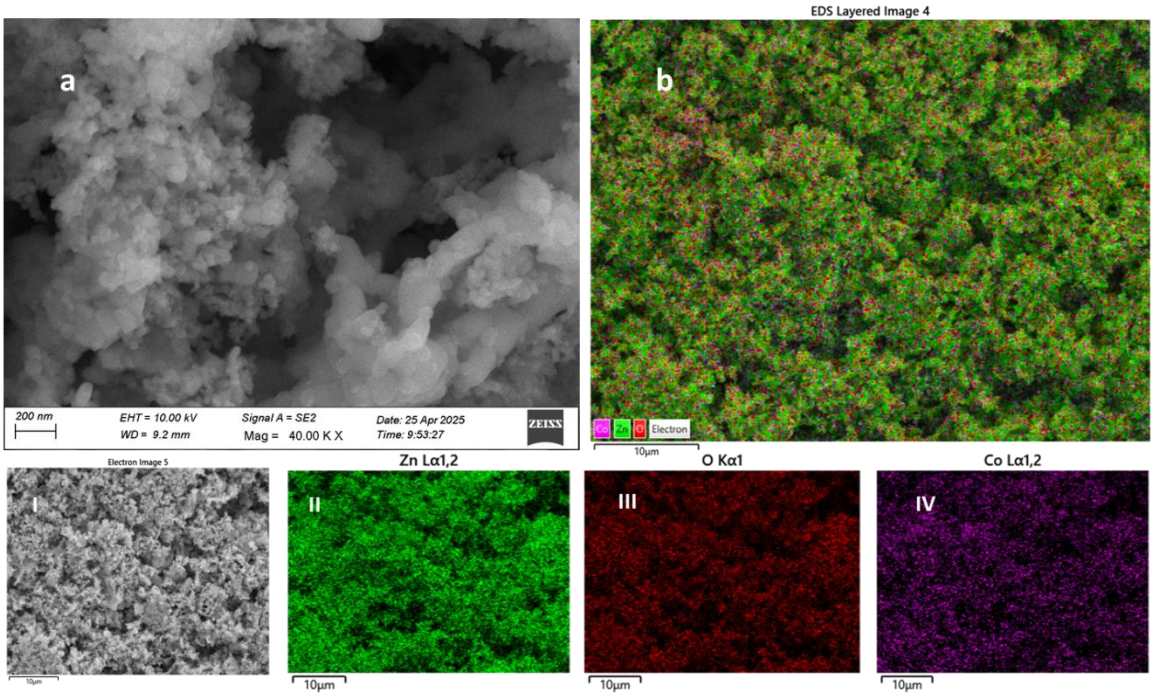


The morphological and elemental distribution analysis of CZnO heterostructures is displayed in Figure 12. (a) surface features FESEM image; (b) EDS elements distribution map; (I) electron image used for EDS mapping; and (II, III, and IV) elemental mapping for cobalt, oxygen, and zinc, respectively.

Figure 13 depicts the EDX elemental analysis of the CZnO sample. The presence of cobalt peaks in the EDX spectrum demonstrates that cobalt ions were successfully incorporated into the ZnO matrix.. The inset table in the spectrum presents the quantitative analysis, indicating elemental weight percentages of approximately 16.23% for oxygen, 15.65% for cobalt, and 68.13% for zinc. For comparison, Figure 11 displays the EDX results for pure ZnO, which shows elemental compositions of 19.53 wt% oxygen and 80.47 wt% zinc, confirming the expected stoichiometry of undoped ZnO The EDX elemental analysis of the CZnO sample is shown in Figure 13. The successful incorporation of cobalt ions into the ZnO matrix is demonstrated by the presence of cobalt peaks in the EDX spectrum. The quantitative analysis is shown in the spectrum's inset table, which shows elemental weight percentages of roughly 16.23% for oxygen, 15.65% for cobalt, and 68.13% for zinc. For comparison, Figure 11 displays the EDX results for pure ZnO, which shows elemental compositions of 19.53 wt% oxygen and 80.47 wt% zinc, confirming the expected stoichiometry of undoped ZnO

.

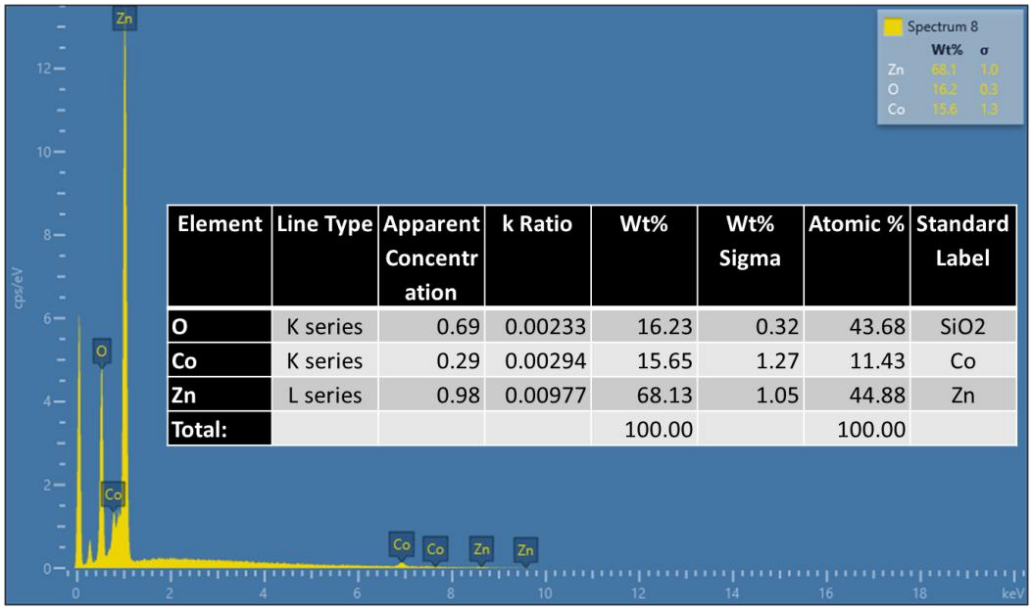


| Element | Line Type | Apparent Concentration | k Ratio | Wt% | Wt% Sigma | Atomic % | Standard Label |
|---|---|---|---|---|---|---|---|
| O | K series | 0.69 | 0.00233 | 16.23 | 0.32 | 43.68 | SiO2 |
| Co | K series | 0.29 | 0.00294 | 15.65 | 1.27 | 11.43 | Co |
| Zn | L series | 0.98 | 0.00977 | 68.13 | 1.05 | 44.88 | Zn |
| Total: | | | | 100.00 | | 100.00 | |

Figure 13 : displays the EDX spectrum used to analyze the elemental composition of the CZnO heterostructure, with a detailed summary of the results presented in the inset table To gain deeper insights into the morphology, particle size, interplanar spacing (d-spacing), and crystallinity—features not clearly distinguishable in the FESEM images—TEM, HRTEM, and SAED techniques were employed. The findings are presented in Figure 14(a–c). The TEM image in Figure 14(a) reveals irregularly shaped particles with noticeable voids on the surface. These voids are likely formed due to the release of gaseous byproducts during the solution combustion synthesis. Based on the scale bar (200 nm), the particle sizes are estimated to range from approximately 20 to 65 nm. High-resolution TEM (HRTEM) analysis confirmed the existence of both ZnO and $CoO_4$ crystalline phases through their measured interplanar distances. Specifically, the d-spacing values of 0.273 nm and 0.241 nm correspond to the (111) plane of ZnO and the (222) plane of $CoO_4$, respectively, as illustrated in Figure 14(b) (Hassaan et al., 2024). The SAED pattern in Figure 14(c) exhibits distinct diffraction rings and spots characteristic of the hexagonal ZnO lattice, confirming the crystalline nature of the synthesized CZnO material.

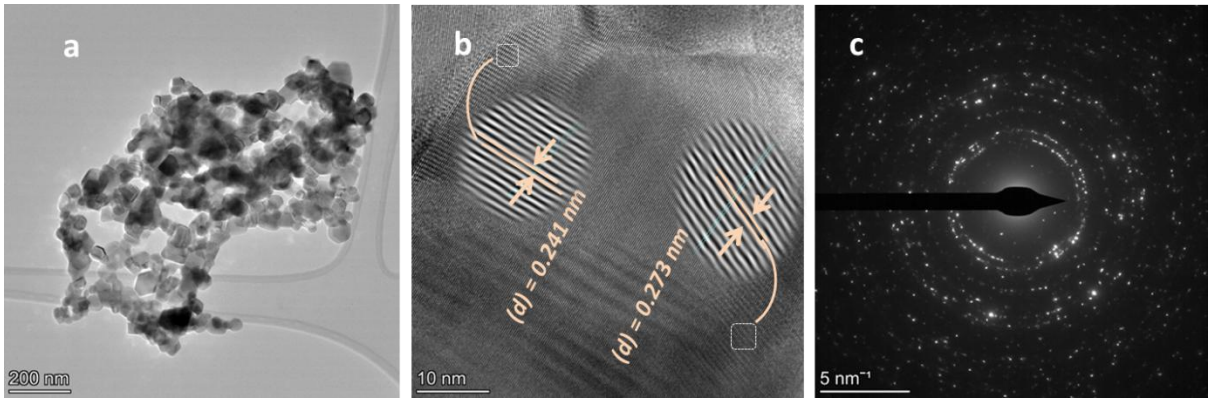


Figure 7. Microscopic morphological investigation of CZnO heterostructure materials: (a–c) the CZnO heterostructure's TEM, HRTEM, and SAED ring pictures, respectively.

### 4.2. Photocatalysis and Mechanism

According to our earlier research on iron and copper co-doped zinc oxide, the ideal values were determined to be 10 mg of catalyst and 10 pH of the solution (Belay et al., 2023). The amount of catalyst has a significant impact on the possibility for material deterioration. . Its quantity rises the number of active sites, which increases the amount of methylene blue dye absorbed. More pollutant adsorption on the catalyst's surface is advantageous since photon-assisted dye degradation occurred there. However, because turbidity is created, increasing the catalyst amount more also prevents the incoming photon. Additionally, the increased catalyst concentration aids in the reduction and agglomeration of the catalyst active sites. (Mirzaeifard et al., 2020). The answer Another major factor influencing methylene blue ionisation and catalyst surface charge is pH. The positively charged methylene blue dye cannot be absorbed because the ZnO or CZnO catalyst surface becomes positively charged in an acidic solution. (Prabakaran & Pillay, 2019). Under alkaline circumstances, however, the catalyst surface becomes negatively charged, promoting the electrostatic attraction of MB molecules and enhancing dye degradation via enhanced adsorption.

In many investigations, measuring the quantity of an unknown dye sample using absorbance-wavelength spectra is either missed or confusing. This study created a calibration curve using known concentrations of methylene blue (4, 8, 12, and 16 ppm), resulting in a $R^2$ of 0.9927. Figure 15(a) shows the absorbance spectra for the standard solutions. This calibration data was utilized to build a linear equation, allowing unknown concentrations to be determined (Figure 15(b)).

Figures 15(c) and 15(d) show the absorbance spectra of ZnO and CZnO samples at different time intervals at the maximum absorption wavelength of 663 nm.. Based on the calibration curve, which had a slope of 0.114 and an intercept of 0.284, the concentrations of the dye at different time points (Ct) were calculated. The degradation performance was further analyzed by plotting Ct/Co and ln(Ct/Co) against time, as shown in Figures 16(a) and 16(b).

From the linear fit of the ln(Ct/Co) vs. time plot, the rate constants (k) were determined to be 0.0312 $min^{-1}$ for ZnO and 0.1407 $min^{-1}$ for CZnO. These results demonstrate the enhanced photocatalytic performance of CZnO over pure ZnO. To evaluate the effectiveness of the synthesized catalyst, its degradation rate constants were compared with those reported in recent literature, as summarized in Table 1. Except for the study by Chatterjee et al.(Chatterjee et al., 2023), this work shows superior rate constants compared to other reports. The current study's catalytic potential is summarised in Table 1 together with recent related literature findings. With the exception of reference 13, which was synthesised using the precipitation method, the rate constant values for this study are nearly higher than those for the other studies, as the table illustrates. But according to the techniques employed, this study is easy to utilise, yields more products, and is economical for usage in scale-up applications.

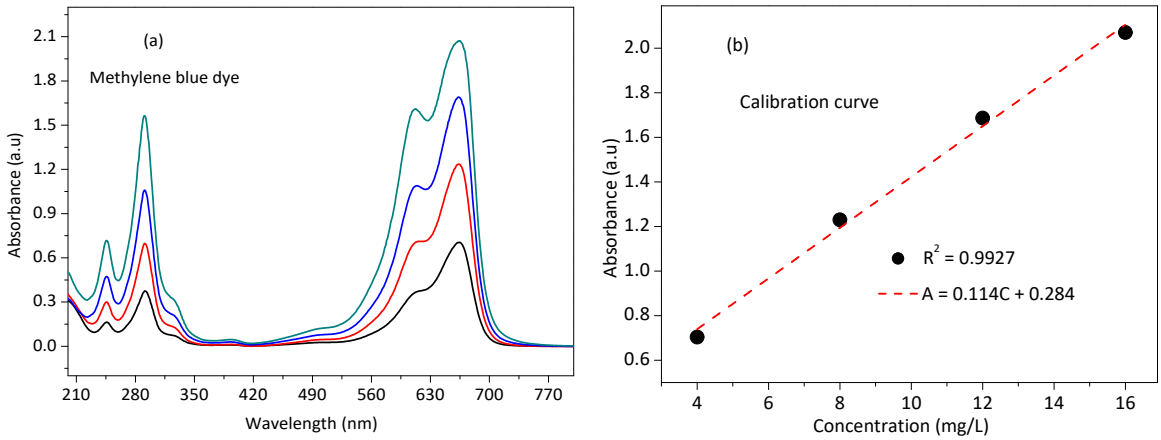

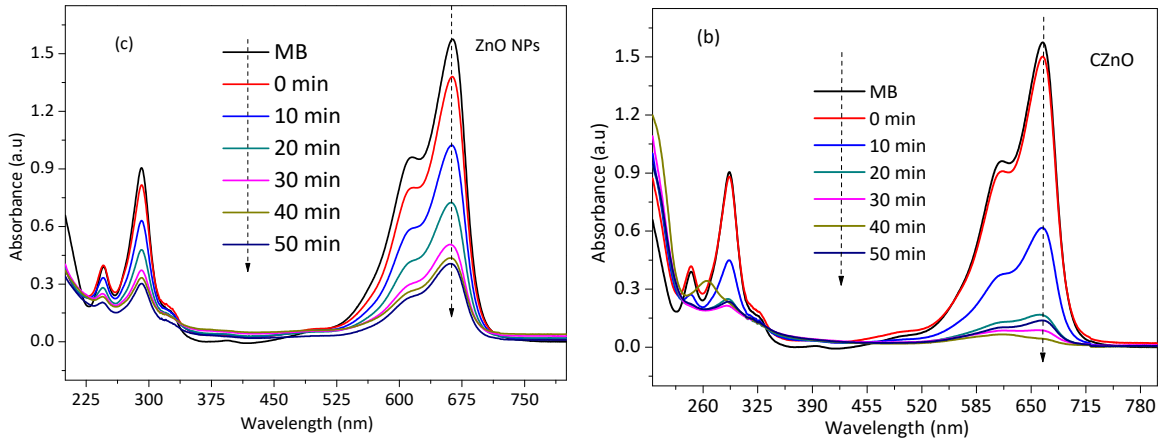


Figure 15: (a) Absorbance spectra of standard methylene blue (MB) dye solutions at concentrations of 4, 8, 12, and 16 ppm, plotted against wavelength (arbitrary units); (b) calibration curve showing the relationship between absorbance and dye concentration (ppm); (c) absorbance spectra of ZnO nanoparticles, and (d) CZnO heterostructure during photocatalytic degradation of MB over time. Measurements were taken at 0, 10, 20, 30, 40, and 50 minutes.

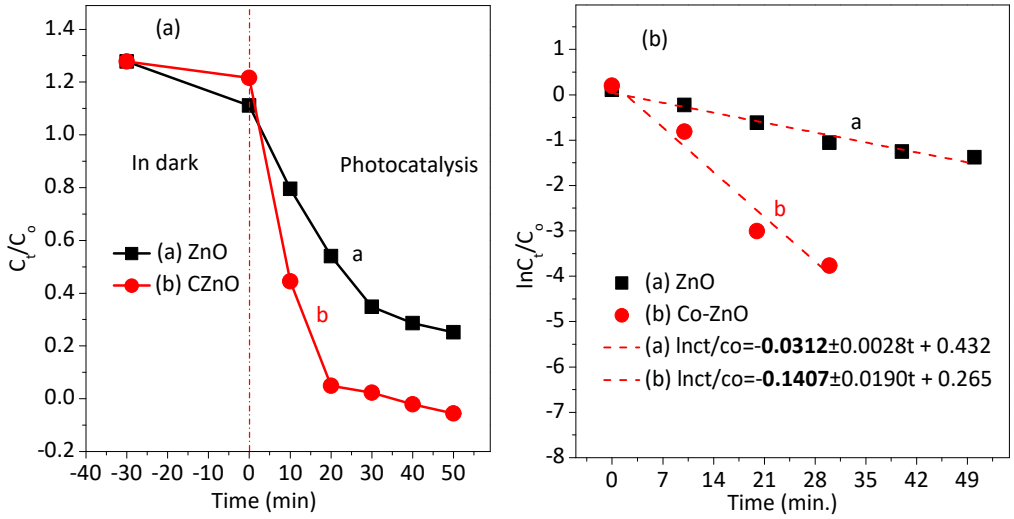


Figure 8: (a) ZnO NPs and CZnO heterostructure test plots of $C_t/C_o$ versus time photocatalysis potential; (b) ZnO NPs and CZnO heterostructure test plots of $\ln C_t/C_o$ versus time.

Based on recent literature reports and the enhanced photocatalysis capability,

Figure 17 presents a schematic representation of the proposed degradation mechanism, drawing from recent literature and the observed improvement in photocatalytic activity. In inset (a) of Figure 17, the doping process is shown to introduce localized defect states between the valence band (VB) and conduction band (CB) of ZnO. These defect levels enhance photocatalytic activity by serving as donor or acceptor sites and facilitating d–d

transitions, which help inhibit electron–hole recombination. Specifically, donor-type transitions involve electron excitation from $Co^{2+}$ or $Co^{3+}$ to the CB of ZnO, while acceptor-type transitions involve electron transfer from $Co^{2+}$ or $Co^{+}$ to the VB of ZnO [4].

Several studies (Alshaikh et al., 2021; Markhabayeva et al., 2023; Mohamed Reda et al., 2017), ZnO has a higher negative conduction band edge prior to contact than $Co_3O_4$, whereas its valence band edge potential is more positive than $Co_3O_4$. This indicates that prior to contact; the $CoO_4$ had a greater work function than ZnO. Consequently, for ZnO and $CoO_4$, the Fermi level shift shifts downward and upward, respectively. Because of this Fermi level shift, ZnO has a lower charge density and $CoO_4$ has a greater negative charge density.

Kim et al. (Kim et al., 2017) reported a similar heterojunction interpretation between ZnO and $CoO_4$ for the ciprofloxacin oxidation application. As illustrated in Figure 17 (inset label b, heterojunction), the generated potential difference causes the electron to migrate from $CoO_4$ to ZnO and the holes to migrate from ZnO to $CoO_4$. This movement of electrons and holes improves the process of charge transfer and stops recombination.

*Table 1.* This work's photocatalytic degradation capabilities are compared with other recent publications in relevant literature.

| Materials | Method used | Precursors used | Properties change due to doping | Bandgap (eV) | Pollutant used, time and conc. | Rate constant | Ref. |
|---|---|---|---|---|---|---|---|
| Zinc oxide doped with cobalt | Sol-gel | $Zn(CH_3CO_2)_2 \cdot 2H_2O$ and $Co(CH_3CO_2)_2 .4H_2O$ | Not much optical properties change observed | 3.37 | 40 minutes of methylene blue and 90 minutes of the antibiotic ciprofloxacin at a dose of 30 mg/L 180 minutes, 10 mg/L of methyl orange dye | 0.0857 $min^{-1}$ | (Oukacha et al., 2024) |
| Zinc oxide doped with cobalt | co-precipitation | $Zn(CH_3CO_2)_2 \cdot 2H_2O$ and $Co(CH_3CO_2)_2 .4H_2O$ | Electron-hole recombination hindrance | 2.75 | 40 minutes of methylene blue and 90 minutes of the antibiotic ciprofloxacin at a dose of 30 mg/L | 0.0387 $min^{-1}$ | (Meky et al., 2025) |
| Zinc oxide doped with cobalt | Chemical vapor deposition | $Zn(C_5H_7O_2)_2$ and $Co(C_5H_7O_2)_2$ | Suppressed emission due to doping | - | 0.0025 $min^{-1}$ | (Karpyna et al., 2024) | |
| Zinc oxide - doped with cobalt | Green (*Nelumbo nucifera* leaf extract) | $Zn(NO_3)_2 \cdot 6H_2O$ and $Co(NO_3)_2 \cdot 6H_2O$ | Showed enhanced optical property improvements | 2.57 | Rhodamine B, 140 min, | 0.0098 $min^{-1}$ | (Naveenkumar et al., 2024) |
| Zinc oxide - doped with cobalt | Hydrothermal | - | $Co^{2+}/Co^{3+}$ inclusion in the ZnO lattice and changing the optical properties | Not much bandgap change was observed | Fluoxetine, Ofloxacin and diclofenac sodium | 0.061 $min^{-1}$ | (Hassaan et al., 2024) |
| Zinc oxide doped with cobalt | Wet impregnation | ZnO NPs and $Co(NO_3)_2 . 6H_2O$ | Positive and negative correction and ZnO's bandgap shrinkage | Not much bandgap change was observed | p-nitrophenol, 180 min, a 30 mg/L | - | (Akhtar et al., 2023) |
| Cobalt-doped zinc oxide | Wet-precipitation | $Zn(CH_3CO_2)_2 \cdot 2H_2O$ and $CoCl_2$ | Optical property improvement | 2.99 | Methylene blue, 5 min, a 10 mg/L | 0.43 $min^{-1}$ | (Chatterjee et al., 2023) |
| $Co_3O_4$/ZnO heterojunctions | one-pot sol–gel | $Zn(NO_3)_2 \cdot 6H_2O$ and $Co(NO_3)_2 \cdot 6H_2O$ | Charge transfer due to p-n heterojunction inhibition | 2.53 | Ciprofloxacin oxidation, | 0.2 $min^{-1}$ | (Alshaikh et al., 2021) |
| Co-ZnO/$Co_3O_4$ | Facile solid-state | $Zn(CH_3CO_2)_2 \cdot 2H_2O$ | Inhibiting electron- | - | Rhodamine B, 60 min, | 0.0336 | (Mohamed Reda et al., 2017) |

| | | | | | | |
|---|---|---|---|---|---|---|
| heterojunctions | reaction | and $Co(CH_3CO_2)_2$ .$4H_2O$ | hole recombination | 5 mg/L | $min^{-1}$ | |
| Co-ZnO/$Co_3O_4$ heterostructure | Sol-gel autocombustion | Zn(CH3CO2).$2H_2O$ and $(NO_3)_2 \cdot 6H_2O$ | Bandgap and charger transport | 1.73 | Methylene blue, 50 min, a 10 mg/L | 0.141 $min^{-1}$ | This study |

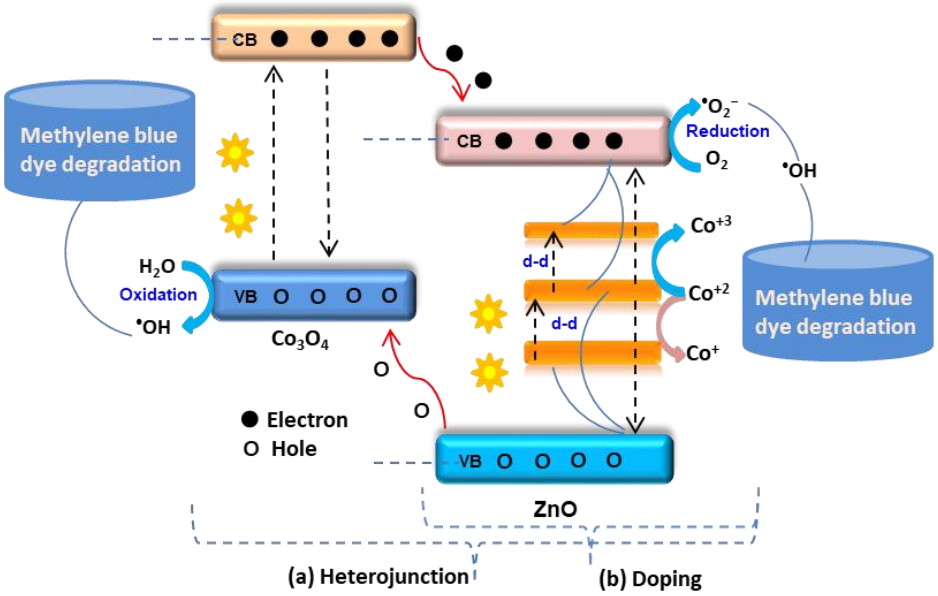


Figure 9: suggested potential mechanism for the formation of heterojunctions between ZnO and $CoO_4$ and the inclusion of cobalt in the ZnO crystal.

## 5. Conclusions

In conclusion, a straightforward sol-gel and autocombustion method was used to successfully synthesise Co-ZnO/$Co_3O_4$. The peak shift in the XRD pattern verified that cobalt ions were present in the zinc oxide crystals. The formation of a ZnO/$Co_3O_4$ heterojunction was evidenced by a distinct peak unrelated to any known crystalline phase in the XRD pattern, as well as by d-spacing measurements obtained from HRTEM analysis. Compared to pure ZnO nanoparticles, the Co-ZnO sample exhibited a smaller average crystallite size (10.7 nm vs. 26.3 nm), indicating a high surface area for the cobalt-containing nanoparticles. TEM imaging showed that the particles, although agglomerated, remained within the nanoscale range of 20–65 nm. The introduction of cobalt and the creation of interface contact enhanced both the optical absorption range and the charge transfer efficiency. The broad spectrum absorption and electron transfer charactersics were improved by the addition of cobalt and the development of interfacial contact. ZnO and CZnO have indirect bandgap energies of 3.05 and 1.71 eV, respectively. Charge transfer across the dopant level and interfacial contact was demonstrated by the fact that the PL spectrum intensity for CZnO was nearly nil emission in comparison to ZnO. The FESEM-EDS study verified the cobalt's excellent distribution and agglomerated surface morphology on the ZnO host surface. Model methylene blue dye was determined to examine the effects of heterojunction potential and dopant incorporation. Compared to ZnO ($k = 0.031\ min^{-1}$), CZnO has a roughly 4.5-fold higher degradation potential ($k = 0.141\ min^{-1}$). Therefore, it is feasible to draw the conclusion that the straightforward combustion method and readily synthesised porous material can be evaluated and applied in extensive .

## References


Abebe, B., Gupta, N. K., & Tsegaye, D. (2024). A critical mini-review on doping and heterojunction formation in ZnO-based catalysts. *RSC Advances*, *14*(25), 17338–17349. https://doi.org/10.1039/D4RA02568G

Akhtar, A., Akram, K., Aslam, Z., Ihsanullah, I., Baig, N., & Bello, M. M. (2023). Photocatalytic degradation of p-nitrophenol in wastewater by heterogeneous cobalt supported <scp>ZnO</scp> nanoparticles: Modeling and optimization using response surface methodology. *Environmental Progress & Sustainable Energy*, *42*(2). https://doi.org/10.1002/ep.13984

Ali, S., Ismail, P. M., Khan, M., Dang, A., Ali, S., Zada, A., Raziq, F., Khan, I., Khan, M. S., Ateeq, M., Khan, W., Bakhtiar, S. H., Ali, H., Wu, X., Shah, M. I. A., Vinu, A., Yi, J., Xia, P., & Qiao, L. (2024). Charge transfer in TiO 2 -based photocatalysis: fundamental mechanisms to material strategies. *Nanoscale*, *16*(9), 4352–4377. https://doi.org/10.1039/D3NR04534J

Alshaikh, H., Shawky, A., Mohamed, R. M., Knight, J. G., & Roselin, L. S. (2021). Solution-based synthesis of Co3O4/ZnO p-n heterojunctions for rapid visible-light-driven oxidation of ciprofloxacin. *Journal of Molecular Liquids*, *334*, 116092. https://doi.org/10.1016/j.molliq.2021.116092

Balapure, A., Ray Dutta, J., & Ganesan, R. (2024). Recent advances in semiconductor heterojunctions: a detailed review of the fundamentals of photocatalysis, charge transfer mechanism and materials. *RSC Applied Interfaces*, *1*(1), 43–69. https://doi.org/10.1039/D3LF00126A

Barick, K. C., Singh, S., Aslam, M., & Bahadur, D. (2010). Porosity and photocatalytic studies of transition metal doped ZnO nanoclusters. *Microporous and Mesoporous Materials*, *134*(1–3), 195–202. https://doi.org/10.1016/j.micromeso.2010.05.026

Belay, H., Abebe, B., Tsegaye, D., Ravikumar, C. R., Reddy, S. G., & Ananda Murthy, H. C. (2023). Chemistry of iron and copper co-doped zinc oxide: reduction and degradation of pollutants. *Catalysis Science & Technology*. https://doi.org/10.1039/D3CY00516J

Chatterjee, K., Dutta, A., Mishra, S., Bairy, B., Sen, M. B., Gorai, A., Saha, S. K., & Akhtar, A. J. (2023). Impact of tailoring of the defect states and the band gap towards extreme photocatalytic performance and photo-induced conductivity in cobalt doped ZnO QD. *Ceramics International*, *49*(20), 32768–32778. https://doi.org/10.1016/j.ceramint.2023.07.245

Dagareh, M. I., Hafeez, H. Y., Mohammed, J., Kafadi, A. D. G., Suleiman, A. B., & Ndikilar, C. E. (2024). Current trends and future perspectives on ZnO-based materials for robust and stable solar fuel (H2) generation. *Chemical Physics Impact*, *9*(1–3), 100774. https://doi.org/10.1016/j.chphi.2024.100774

Deshapriya, S. D., & Munaweera, I. (2024). Visible-Light-Active Electrospun Membranes Based on Cobalt-Doped ZnO Nanohybrids: Applications for Food Packaging. *ChemistrySelect*, *9*(9). https://doi.org/10.1002/slct.202303830

Domingues, L., Jayakrishnan, A. R., Kaim, A., Gwozdz, K., Istrate, M. C., Ghica, C., Pereira, M., Castro, A., Marques, L., Hoye, R. L. Z., MacManus-Driscoll, J. L., & Silva, J. P. B. (2024). Tri-layered Si/Co3O4/ZnO heterojunction for high-performance visible photodetection. *Journal of Materials Chemistry C*, *12*(24), 8727–8736. https://doi.org/10.1039/d4tc01624f

Gao, Y., Meng, F., Li, X., Wen, J. Z., & Li, Z. (2016). Factors controlling nanosized Ni–Al 2 O 3 catalysts synthesized by solution combustion for slurry-phase CO methanation: the ratio of reducing valences to oxidizing valences in redox systems. *Catalysis Science & Technology*, *6*(21), 7800–7811. https://doi.org/10.1039/C6CY01603K

Goncharuk, V. V., Bagrii, V. A., Mel'nik, L. A., Chebotareva, R. D., & Bashtan, S. Y. (2010). The use of redox potential in water treatment processes. *Journal of Water Chemistry and Technology*, *32*(1), 1–9. https://doi.org/10.3103/S1063455X10010017

Hassaan, M. A., Meky, A. I., Fetouh, H. A., Ismail, A. M., & El Nemr, A. (2024). Central composite design and mechanism of antibiotic ciprofloxacin photodegradation under visible light by green hydrothermal synthesized cobalt-doped zinc oxide nanoparticles. *Scientific Reports*, *14*(1), 9144. https://doi.org/10.1038/s41598-024-58961-4

Irede, E. L., Awoyemi, R. F., Owolabi, B., Aworinde, O. R., Kajola, R. O., Hazeez, A., Raji, A. A., Ganiyu, L. O., Onukwuli, C. O., Onivefu, A. P., & Ifijen, I. H. (2024). Cutting-edge developments in zinc oxide nanoparticles: synthesis and applications for enhanced antimicrobial and UV protection in healthcare solutions. *RSC Advances*, *14*(29), 20992–21034. https://doi.org/10.1039/D4RA02452D

Ji, H., Cai, C., Zhou, S., & Liu, W. (2018). Structure, photoluminescence, and magnetic properties of Co-doped ZnO nanoparticles. *Journal of Materials Science: Materials in Electronics*, *29*(15), 12917–12926. https://doi.org/10.1007/s10854-018-9411-7

Kaphle, A., & Hari, P. (2017). Variation of index of refraction in cobalt doped ZnO nanostructures. *Journal of Applied Physics*, *122*(16), 165304. https://doi.org/10.1063/1.5001713

Karamat, A., Khan, M. I., Mujtaba, A., Atif, M., Zar Muaawia, A., Flores-Valenzuela, J., Ali, B., Shahid, W., & Hussain, S. (2024). Revolutionizing photocatalysis: Synergistic enhancement of structural, optical, and photodegradation properties in Be-doped V2O5 nanoparticles for efficient methylene blue removal. *Results in Chemistry*, *8*(4), 101600. https://doi.org/10.1016/j.rechem.2024.101600

Karpyna, V., Myroniuk, L., Myroniuk, D., Bykov, O., Olifan, O., Kolomys, O., Strelchuk, V., Bugaiova, M., Kovalchuk, I., & Ievtushenko, A. (2024). Effect of Cobalt Doping on Structural, Optical, and Photocatalytic Properties of ZnO Nanostructures. *Catalysis Letters*, *154*(5), 2503–2512. https://doi.org/10.1007/s10562-023-04493-x

Keshari, A. K., Gupta, P., & Singh, M. (2021). ZnO nanoparticles doping with transition metal elements in polymeric and biomacromolecular matrix and their optical evolution. *Optical Materials*, *111*(3), 110697. https://doi.org/10.1016/j.optmat.2020.110697

Khan, I., Saeed, K., & Khan, I. (2019). Nanoparticles: Properties, applications and toxicities. *Arabian Journal of Chemistry*, *12*(7), 908–931. https://doi.org/10.1016/j.arabjc.2017.05.011

Khort, A., Hedberg, J., Mei, N., Romanovski, V., Blomberg, E., & Odnevall, I. (2021). Corrosion and transformation of solution combustion synthesized Co, Ni and CoNi nanoparticles in synthetic freshwater with and without natural organic matter. *Scientific Reports*, *11*(1), 7860. https://doi.org/10.1038/s41598-021-87250-7

Kim, J.-W., Lee, S. J., Biswas, P., Lee, T. Il, & Myoung, J.-M. (2017). Solution-processed n -ZnO nanorod/ p -Co 3 O 4 nanoplate heterojunction light-emitting diode. *Applied Surface Science*, *406*, 192–198. https://doi.org/10.1016/j.apsusc.2017.02.129

Leimane, M., Laganovska, K., Vītola, V., Dile, M., Križmane, K., Tunēns, G., & Zolotarjovs, A. (2025). Effect of alkali metal ion doping on the optical and morphological properties of translucent $SiO_2$ pellets. *Next Materials*, *8*(3), 100929. https://doi.org/10.1016/j.nxmate.2025.100929

Liu, B., You, Y., Zhang, H., Wu, H., Jin, J., & Liu, H. (2016). Synthesis of ZnO nano-powders via a novel PVA-assisted freeze-drying process. *RSC Advances*, *6*(111), 110349–110355. https://doi.org/10.1039/C6RA24154A

Luo, H., Chen, J., Wang, J., Li, S., Li, X., & Yang, J. (2025). Facile boosting catalytic thermal decomposition of ammonium perchlorate from 3D porous nano Co3O4@ZnO composites. *Fuel*, *379*(July 2024), 133122. https://doi.org/10.1016/j.fuel.2024.133122

Markhabayeva, A. A., Kalkozova, Z. K., Nemkayeva, R., Yerlanuly, Y., Anarova, A. S., Tulegenova, M. A., Tulegenova, A. T., & Abdullin, K. A. (2023). Construction of a ZnO Heterogeneous Structure Using Co3O4 as a Co-Catalyst to Enhance Photoelectrochemical Performance. *Materials*, *17*(1), 146. https://doi.org/10.3390/ma17010146

Meky, A. I., Hassaan, M. A., El-Nemr, M. A., Fetouh, H. A., Ismail, A. M., & El Nemr, A. (2025). Kinetics, central composite design and artificial neural network modelling of ciprofloxacin antibiotic photodegradation using fabricated cobalt-doped zinc oxide nanoparticles. *Scientific Reports*, *15*(1), 1610. https://doi.org/10.1038/s41598-024-84568-w

Meky, A. I., Hassaan, M. A., Fetouh, H. A., Ismail, A. M., & El Nemr, A. (2024). Hydrothermal fabrication, characterization and RSM optimization of cobalt-doped zinc oxide nanoparticles for antibiotic photodegradation under visible light. *Scientific Reports*, *14*(1), 2016. https://doi.org/10.1038/s41598-024-52430-8

Mirzaeifard, Z., Shariatinia, Z., Jourshabani, M., & Rezaei Darvishi, S. M. (2020). ZnO Photocatalyst Revisited: Effective Photocatalytic Degradation of Emerging Contaminants Using S-Doped ZnO

Nanoparticles under Visible Light Radiation. *Industrial & Engineering Chemistry Research*, *59*(36), 15894–15911. https://doi.org/10.1021/acs.iecr.0c03192

Mohamed Reda, G., Fan, H., & Tian, H. (2017). Room-temperature solid state synthesis of Co 3 O 4 /ZnO p–n heterostructure and its photocatalytic activity. *Advanced Powder Technology*, *28*(3), 953–963. https://doi.org/10.1016/j.apt.2016.12.025

Naveenkumar, R., Karthikeyan, B., & Senthilvelan, S. (2024). Photocatalytic Degradation of Toxic Rhodamine B Dye by Green-Synthesised Activated Carbon-Supported Cobalt Doped ZnO With Further Assessment of ZnO Nanoparticles in Antimicrobial Applications. *ChemistrySelect*, *9*(29). https://doi.org/10.1002/slct.202401448

Nguyen, K. Q., Nguyen, H. T., Bui, T. K., Nguyen, T.-T., & Pham, V. Van. (2024). Straightforward electrochemical synthesis of a Co 3 O 4 nanopetal/ZnO nanoplate p–n junction for photoelectrochemical water splitting. *Nanoscale Advances*, *6*(16), 4167–4179. https://doi.org/10.1039/D4NA00036F

Oukacha, K., El-Yahyaoui, A., Laânab, L., EL Hajjaji, S., & Jaber, B. (2024). Optimization of Cobalt Doping Content for the Synthesis of High-performance Photocatalytic Co-ZnO Nanoparticles. *Journal of Inorganic and Organometallic Polymers and Materials*. https://doi.org/10.1007/s10904-024-03488-4

Prabakaran, E., & Pillay, K. (2019). Synthesis of N-doped ZnO nanoparticles with cabbage morphology as a catalyst for the efficient photocatalytic degradation of methylene blue under UV and visible light. *RSC Advances*, *9*(13), 7509–7535. https://doi.org/10.1039/C8RA09962F

Qu, B., Xiao, Z., & Luo, Y. (2025). Sustainable nanotechnology for food preservation: Synthesis, mechanisms, and applications of zinc oxide nanoparticles. *Journal of Agriculture and Food Research*, *19*(1), 101743. https://doi.org/10.1016/j.jafr.2025.101743

Raha, S., & Ahmaruzzaman, M. (2022). ZnO nanostructured materials and their potential applications: progress, challenges and perspectives. *Nanoscale Advances*, *4*(8), 1868–1925. https://doi.org/10.1016/j.talanta.2018.12.034

Ren, K., Wang, K., Cheng, Y., Tang, W., & Zhang, G. (2020). Two-dimensional heterostructures for photocatalytic water splitting: a review of recent progress. *Nano Futures*, *4*(3), 032006. https://doi.org/10.1088/2399-1984/abacab

Singh, K., Nancy, Kaur, H., Sharma, P. K., Singh, G., & Singh, J. (2023). ZnO and cobalt decorated ZnO NPs: Synthesis, photocatalysis and antimicrobial applications. *Chemosphere*, *313*(1–3), 137322. https://doi.org/10.1016/j.chemosphere.2022.137322

Tien, T.-M., & Chen, E. L. (2023). A Novel ZnO/Co3O4 Nanoparticle for Enhanced Photocatalytic Hydrogen Evolution under Visible Light Irradiation. *Catalysts*, *13*(5), 852. https://doi.org/10.3390/catal13050852

Vieii, F. H., Havigh, R. S., & Chenari, H. M. (2025). Electrospun preparation of nickel and Cobalt-doped ZnO fibers: study on the physical properties. *Scientific Reports*, *15*(1), 10898. https://doi.org/10.1038/s41598-025-95443-7

Wachs, I. E. (1996). Raman and IR studies of surface metal oxide species on oxide supports: Supported metal oxide catalysts. *Catalysis Today*, *27*(3–4), 437–455. https://doi.org/10.1016/0920-5861(95)00203-0

Wei, B., Zhang, J., Lin, L., Wu, T., Cheng, Z., Ma, Y., Li, J., & Yu, S. (2024). Enhancing Electrical Transport Performance of Polycrystalline Tin Selenide by Doping Different Elements. *Physica Status Solidi (A)*, *221*(9), 21–28. https://doi.org/10.1002/pssa.202300717

Yakushova, N. D., Gubich, I. A., Karmanov, A. A., Komolov, A. S., Koroleva, A. V., Korotcenkov, G., & Pronin, I. A. (2025). Photocatalytic Degradation of Toxic Dyes on Cu and Al Co-Doped ZnO Nanostructured Films: A Comparative Study. *Technologies*, *13*(7), 277. https://doi.org/10.3390/technologies13070277

Yang, W., Ullah, I., Jiang, Z.-G., Neder, R. B., & Zhan, C.-H. (2025). Tailoring ultra-small ZnO nanoparticles through cobalt doping to enhance photocatalytic CO 2 reduction. *RSC Advances*, *15*(15), 11934–11941. https://doi.org/10.1039/D5RA01374G